Design of deep supported excavations: comparison between real behavior and predictions based on the subgrade coefficient method

Tomasz Daktera, Emmanuel Bourgeois, Pierre Schmitt, Thierry Jeanmaire, Laure Delva, Grégoire Priol

Proceedings of the XVII ECSMGE-2019
Geotechnical Engineering foundation of the future
ISBN 978-9935-9436-1-3

doi: 10.32075/17ECSMGE-2019-0495

XVII European Conference
ECSMGE 2019
Reykjavík
on Soil Mechanics
and Geotechnical Engineering

Design of deep supported excavations: comparison between real behavior and predictions based on the subgrade coefficient method

Conception de fouilles profondes : comparaison entre comportement réel et prédictions basées sur la méthode du coefficient de réaction

Tomasz Daktera
Soletanche Bachy, IFSTTAR, Paris, France

Emmanuel Bourgeois
IFSTTAR, Champs-sur-Marne, France

Pierre Schmitt, Thierry Jeanmaire, Laure Delva
Soletanche Bachy, Rueil-Malmaison, France

Grégoire Priol
Société du Grand Paris, Saint-Denis, France

ABSTRACT: The stations of the line 15 of the Grand Paris Express include diaphragm walls 50 m deep with excavation depths over 30 m. Their behavior at "Les Ardoines" metro station has been carefully monitored during the excavation process by inclinometers in diaphragm walls, strain gauges on steel props and topographic monitoring. A complete analysis of the monitoring data has been performed, especially for the steel propping system where the earth-induced and temperature-induced loads have been separated. The aim of this work is to improve the methodology of determination of the parameters of the subgrade reaction coefficient. Comparison with finite element simulations will also provide an opportunity to improve consistency between the parameters used in both methods.

RÉSUMÉ : Les gares de la ligne 15 du Grand Paris Express comportent des parois moulées de plus de 50 m de profondeur et plus de 30 m de profondeur excavée. Leur comportement pendant les étapes d'excavation à la station « Les Ardoines » a fait l'objet d'une instrumentation détaillée : mesures inclinométriques pour suivre les déformations des parois moulées, jauges de déformation sur les butons métalliques, mesures topographiques classiques. Une analyse complète des données des instrumentations a été faite, en particulier pour les butons métalliques où les efforts induits par la poussée des terres et par la température ont été séparés. Le but de ce travail est d'améliorer la méthodologie de détermination des paramètres de la méthode du coefficient de réaction. La comparaison des mesures avec des modélisations par éléments finis permettra également d'améliorer la cohérence entre les paramètres utilisés dans les deux méthodes.

Keywords: diaphragm wall, field testing & monitoring, temporary works, subgrade reaction coefficient

1 INTRODUCTION

The Grand Paris Express is the largest infrastructure project currently under construction in Europe. This megaproject consists of over 200 kilometers of automatic metro lines (mostly tunnels built with TBMs) and 68 stations. This paper focuses on the station of Les Ardoines, on the South section of line 15, which should be put into service in 2025.

The TBM will bore through the station after a complete excavation. Figure 1 shows the excavation works in July 2018.

Figure 1. Les Ardoines metro station during the excavation stage – 25m of excavation

2 LES ARDOINES METRO STATION

2.1 General structure's information

The station is enclosed within a 112 m long and 31.2 m wide rectangle made of diaphragm walls. It is divided into two "pits", called Western and Eastern pits, separated by a diaphragm wall. This article focuses on the Western pit construction only. During the excavation process, the wall is supported by three levels of steel props. An additional prop level holds the intermediate diaphragm wall that stands in between both pits. A cross-section of the Western Pit and a top view of the diaphragm walls are shown on Figure 2 and Figure 3. After the construction of the diaphragm walls of both pits, the Eastern Pit has been excavated to 26.15NGF (cantilever).

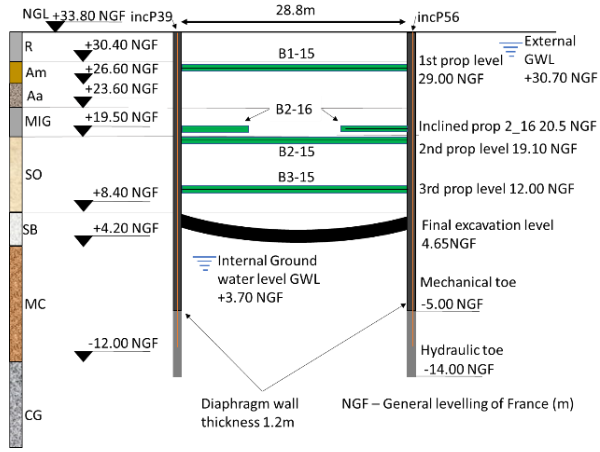

Figure 2. Les Ardoines Western Pit cross section between inclinometers incP39 and incP56

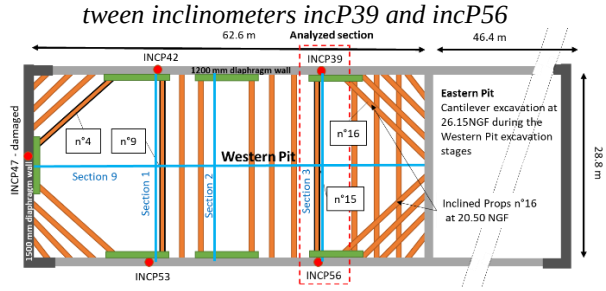

Figure 3. Les Ardoines top view

Then, the construction stages for the Western pit were as follows: 1. Cantilever excavation to 28.4NGF; 2. Prop installation at 29NGF; 3. Excavation to 18.5NGF; 4. Prop installation at 19.1NGF and at 20.5NGF; 5. Excavation to 11.4NGF; 6. Prop installation at 12NGF; 7. excavation to 4.65NGF.

2.2 Geotechnical parameters

The geotechnical study for this project consisted of laboratory tests (classification tests, triaxial drained and undrained tests and other) as well as in-situ pressuremeter tests (PMT). For the back-analysis, an objective study of all geotechnical data available was performed. Such a study allows to understand the reliability of the parameters and their potential heterogeneity and to obtain a representative profile for the analyzed cross-section. The chosen soil parameters are shown in Table 1 where E_M and α are Ménard's modulus and rheological coefficient.

Layer name	code	φ' (°)	c' (kPa)	E_M (MPa)	α (-)
Fill	R	32	10	10.5	0.5
Clayey Sand	Am	37	10	12	0.5
Silica Sand	Aa	37	8	26	0.33
Marl	MIG	36	22	20	0.67
St Ouen Limestone	SO	30	25	78	0.5
Beauchamp Sand	SB	29	31	65	0.5
Marls and Stones	MC	34	61	151	0.5
Hard Limestone	CG	40	100	385	0.5

Table 1. Geotechnical parameters for Les Ardoines

2.3 Instrumentation of Les Ardoines metro station – Western Pit

The monitoring program of the site is composed of the following items: 5 inclinometer tubes within the diaphragm walls, 24 thermally matched vibrating wire strain gauges, installed on 8 steel props on three different levels (n°4, 9, 15) and 12 convergence measurements at three levels over four cross-sections on the diaphragm walls, to measure the horizontal displacements. The monitored elements are shown on Figure 1-3.

3 STRAIN GAUGES ON STEEL PROPS ANALYSIS

The position of the strain gauges must be taken into account in the analysis. On the instrumented circular props, three strain gauges were placed at the uppermost point and at 120 degrees on each side. The mean value of the three strain gauges gives the mean normal stress in the section. The strain gauges were installed 5 prop diameters away from the diaphragm wall in order to avoid the connection's influence (Twine 1999).

3.1 The temperature-induced force

3.1.1 Temperature effects – generalities

Because of thermal expansion, a change in temperature affects the normal force in the prop (unless the ends of the prop are free to move, which is not the case). For a fully restrained prop (where no increase in length is possible), the load difference due to temperature variation is:

$$\Delta P_{temp} = \beta \cdot \Delta T \cdot E \cdot A \qquad (1)$$

where β (K^{-1}), E (MPa) and A (m^2) are the thermal expansion coefficient, Young's modulus and cross-sectional area of the prop and ΔT (°K) is the difference between the current and installation temperature. A prop placed between two diaphragm walls is not fully restrained, thus the prop load variation due to temperature changes is lower than the value given by eq. (1).

3.1.2 Separation of earth-induced and temperature-induced loads in props

To separate temperature-induced and earth-induced loads, the method described by Boone (2000) has been adopted. It is illustrated for prop B1-9. Figure 4a) shows the variations of the mean force in the instrumented prop section with time. The red curve is the temperature variation.

Figure 4b) shows a plot of all the measurement points (one measurement every hour) of the incremental temperature vs incremental load in order to understand the dependence between the temperature and the force increase. The colors on both Figure 4a) and b) match. One can distinguish the weekends with an almost perfectly linear elastic behavior (stage 3 orange and 5 dark red) from the workweeks where the earth-induced load increases (stage 2 dark green, 4 gray and 6 yellow) due to excavations. The slope of $\Delta T/\Delta P$ – denoted by m, allows to quantify the dependency between the variables. For B1-9, $m = 45 kN/°C$. For a fully restrained prop: $m_{restrained} = 93.8\ kN/°C$. The earth-induced loads can be estimated by:

$$P_{earth} = P_{measured} - m \cdot \Delta T \qquad (2)$$

For B1-9 the earth-induced load due to the excavation below the first prop level is considered to be 1800 kN. The same analysis has been performed for the other props. The separated loads are shown on Figure 5.

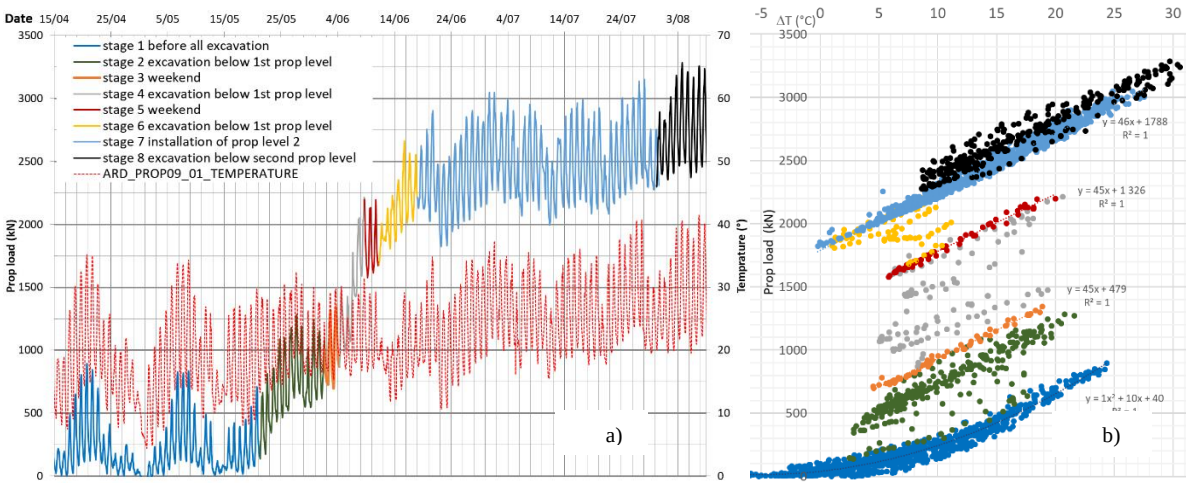

Figure 4.a) Force measured by the strain gauges for B1-9
b) Incremental load change to the incremental temperature change for B1-9

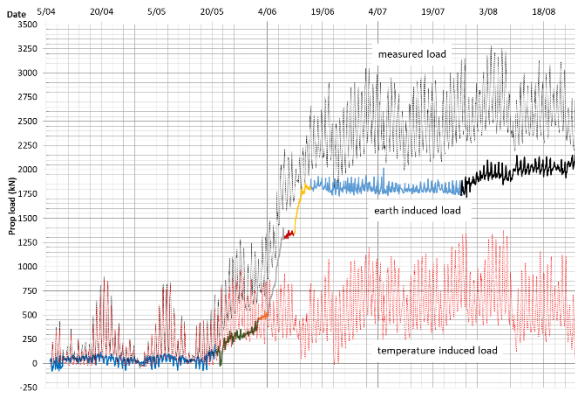

Figure 5. Comparison between the measured load by the strain gauges and the separated earth and temperature-induced loads for prop B1-9

3.1.3 Strain gauges in steel props – conclusions

24 daily temperature and strain values were used for the analysis. The amount of available data allows to distinguish the installation process and separate the temperature and earth-induced stresses. Earth-induced forces should be compared to the forces from Subgrade Reaction Coefficient method (SGRM) or Finite Element Method (FEM) calculations. Table 2 shows the earth induced forces in all 8 struts. The two inclined props (n°4) at the corners of the pit show much lower mean normal force measurements than the straight props. This is interesting as the theoretical stiffness difference between the straight and inclined props does not justify such discrepancies, nor does the distance of the prop to the pits corner (12m) nor arching effects, as most of the applied pressure on the wall consists of water. No explanation of the much lower measured forces is given at this point, but more instrumented inclined props will be analyzed on other deep excavation pits.

Mean force at excavation (kN/m)				
Level	**Prop**	**18.5NGF**	**11.4NGF**	**3.7NGF**
29 NGF	B1-9	320	360	370
	B1-15	290	300	240
19.1 NGF	B2-9	-	1160	1430
	B2-15	-	1460	1200
	B2-4	-	570	690
12 NGF	B3-9	-	-	650
	B3-15	-	-	650
	B3-4	-	-	360

Table 2. Mean earth-induced forces per prop

4 INCLINOMETER READINGS ANALYSIS

Five 45m long inclinometer tubes have been installed within the diaphragm walls, with their toes embedded 5m below the diaphragm wall mechanical toe. Hydraulic toe has also been modeled in both analyses (FEM and SGRM). Initial inclinometer readings were taken before the 27m deep pumping test.

4.1 Subgrade reaction coefficient analysis

The French code on retaining walls (AFNOR 2009), presents two main formulas for the subgrade reaction coefficient k_h determination:

$$k_h = 2.1 \cdot \left(\frac{E_M}{\alpha}\right)^{4/3} / (EI)^{1/3} \quad (3)$$

derived from the more general formula:

$$k_h = K \cdot \left(\frac{E_M}{\alpha}\right) / A \quad (4)$$

where EI (kNm^2) is wall's flexural stiffness, A (m) is a parameter called "interaction depth" and K is considered as 3.6. The diaphragm wall Young's modulus considered in the analysis is 27GPa. Formula (3), also called Schmitt's formula, has shown its validity on regular excavations in France and in the Parisian Region and thus has been used for the excavation stages of the pit (Schmitt 1995, Serrai 2005). According to AFNOR 2009, for the pumping stage formula (4) should be used. For our calculation, the interaction depth A has been considered as the height between the external GWL and the interface between MC and SB layers. Schmitt's formula was used below 4.2NGF.

4.2 FEM analysis

Two FEM simulations have been performed: one with Mohr-Coulomb (Mohr-C) and the other with the Hardening Soil Model (HSM). For the Mohr-C Soil Model, the moduli were (Serrai 2005):

$$E = 4 \cdot E_M / \alpha \quad (5)$$

For the HSM the moduli were:

$$E_{50} = E_{oed} = E_{ur}/3 = 2 \cdot \frac{E_M}{\alpha} \quad (6)$$

The exponent *m* is 0 for all soil layers as the PMT's showed little moduli increase with depth.

4.3 Analysis of pumping test stage

The pumping stage consists of dewatering the pit prior to any excavation. The analysis of this stage is independent of the excavation stages calculations. Four inclinometer curves for this stage are shown on Figure 6a), assuming for comparison purpose that the toe of the inclinometer is fixed. All curves are almost vertical from the bottom to the interface between the MC and SB layers and then leaning forward to a displacement of about 4mm. P56 and P53 inclinometers show inexplicable curvatures above 28NGF and are considered as erroneous measurements.

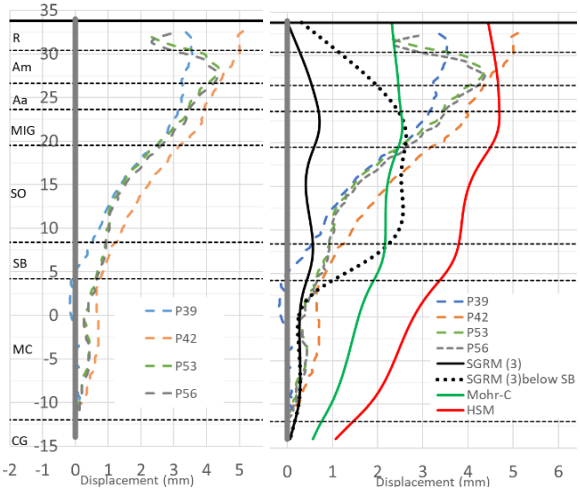

(a) *(b)*

Figure 6. Inclinometer readings for the pumping test with SGRM and FEM (Mohr-C and HSM models)

Calculation results are shown on Figure 6b). With formula (3), the interaction depth is conditioned by the wall's stiffness EI and shows much lower displacements (continuous black curve) than measured. With formula (4), the interaction depth is 27m above the pumping level, to model a translation behavior of the wall. The dotted black curve shows larger displacements, together with a behavior in which the top of the wall seems to be supported. This is not observed on the measured curves. FEM results are represented with green and red curves for Mohr-C and HSM respectively.

Figure 7 presents corrected SGRM and FEM curves in order to obtain a better agreement with the inclinometric measurements. Green and red curves are Mohr-C and HSM calculations respectively, with $E = 6\,E_M/\alpha$ and $E_{50} = 4\,E_M/\alpha$ for the MC and CG soil layers. For the black curves, a k_h increasing with depth was considered to model the dragging of the top layers by the deeper layers which is probably the reason why SGRM conventional calculations in Figure 6 showed an

unrealistic reaction in upper soil layers compared with inclinometer results.

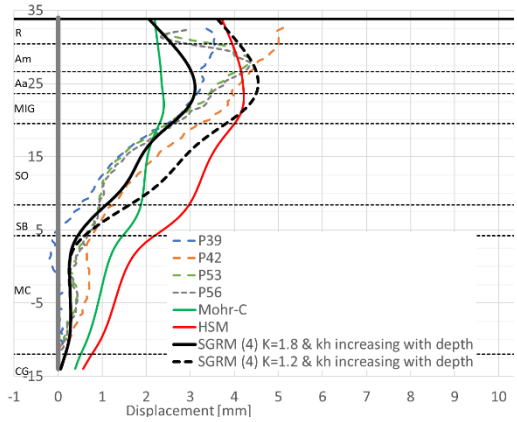

Figure 7. Inclinometer readings for the pumping test with SGRM and FEM corrected models

For both continuous and dashed curves, the interaction depths per layers have been determined as the distance between the layer in question and the lowered water level (3.7NGF). K coefficients of 1.8 and 1.2 have been used respectively. These values account for the fact that the pumping is the primary loading of the soil layers. k_h coefficient in SGRM is defined in a unique way, without distinction between unloading and reloading and thus it is legitimate to change its value for different load paths. For the layers below the pumping level, formula (3) has been used.

The SGRM curves show a much closer fit to the measured ones with variable interaction depths. The FEM models even with artificially higher moduli below the MC and SB interface do not properly model the lower parts of the curves where the measurements show almost no rotation and different curvatures.

4.4 Analysis of the excavations stages

The water level within the excavation has been maintained at 3.7NGF during all excavation stages. The pumping test inclinometer results have been taken as reference for the analysis of the subsequent excavation stages. Formulas (3), (5) and (6) were chosen for the SGRM (as per AFNOR 2009), Mohr-C and HSM models. Figures 8, 9 and 10 compare inclinometric curves and calculations.

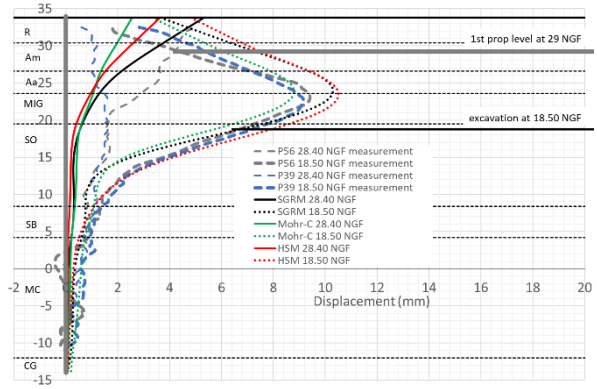

Figure 8. Measurements and calculations for 28.40 NGF and 18.50NGF excavations

The inclinometric curves for the first excavation were not very smooth. SGRM, Mohr-C and HSM models show similar curvatures for both stages shown on Figure 8. Top displacements are 5mm, 2.5mm and 4mm respectively for the 28.4NGF stage. For the excavation stage to 18.5NGF, displacements were slightly overestimated by SGRM and HSM models by less than 2mm. Mohr-C maximum displacement is very close to the measured maximum at about 22.5NGF depth. The displacement curves of the SGRM and Mohr-C models are not as smooth as the measurements or the HSM between 5 and 15NGF.

For the 11.4NGF excavation (see Figure 9), all models show correct curvatures below 5NGF. SGRM's maximum displacement of 14mm is between the maximum of the measured inclinometer 56 and 39 curves. Mohr-C underestimates the maximum displacement by 2mm. HSM shows a good fit for absolute displacements and curvatures below the peak. For the excavation stages at 18.5NGF and 11.4NGF, all models overestimate displacements but give similar curvatures above level 25NGF.

For the final excavation at 4.65NGF, all curves are very similar between 7NGF and the wall toe. The SGRM gives a maximum displacement of 17 mm, between both values measured by the inclinometers. HSM's maximum displacement is just below the measured inc39 –16mm. By

contrast, Mohr-C underestimates the maximum displacement (13mm). All curves have similar shapes above 25NGF.

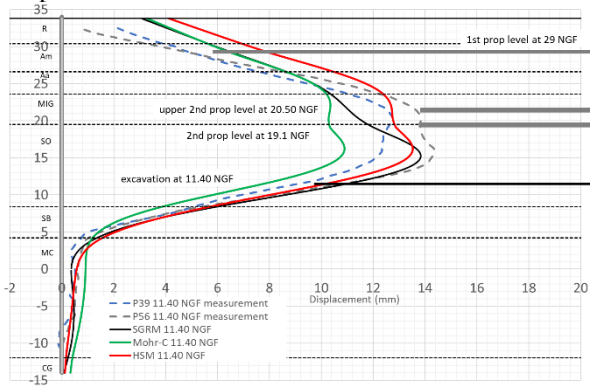

Figure 9. Curves for 11.40NGF excavation

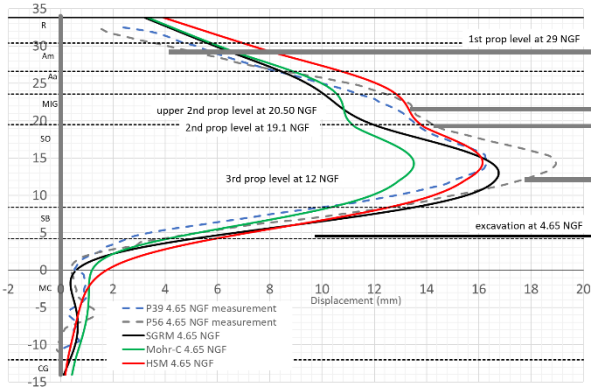

Figure 10. Curves for final excavation 4.65NGF

4.4.1 Prop forces modeling verifications

Since the incremental displacement between inclinometer curves at the prop levels is known, we were able to compare the apparent stiffnesses of the props to theoretical ones. The props' stiffnesses determined from measurements between incP39 and incP56 seem close to theory.

Figures 11 to 13 present the calculated forces for props n°15 and n°9. The analyzed section is the one for props n°15 but props n°9 show interesting behaviors and are presented on the figures as well. Both instrumented props at 29NGF show a different behavior. The force in B1-9 increases for both excavations at 11.40NGF and 4.65NGF. The force in B1-15 increases then decreases as the excavation proceeds. In the SGRM model, the prop force decreases and in the FEM the force increases. Therefore, a conclusion on the behavior cannot be drawn at this point. The SGRM model slightly overestimates prop forces. Mohr-C and HSM both overestimate the prop force and this discrepancy increases with excavation depth.

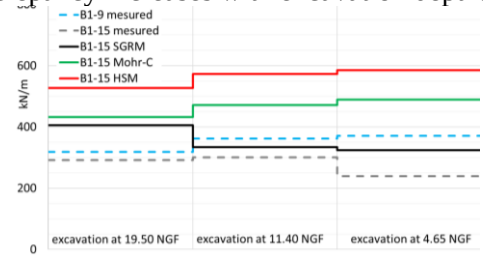

Figure 11. Measured forces for B1-15 and B1-9 compared to SGRM, Mohr-C and HSM

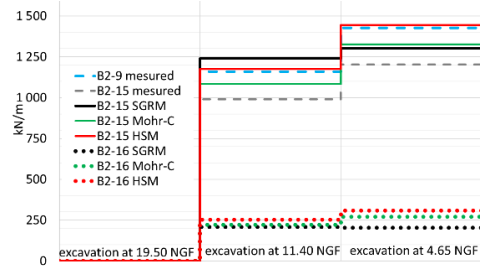

Figure 12. Forces in props at 19.1 and 20.50NGF

The measured prop force in B2-09 is 15% greater than in B2-15 which is probably due to the load taken by the inclined prop B2-16 just above B2-15. SGRM and FEM calculations show that the prop at 20.5NGF supports about 20% of the force of B2-15, which is close to the measured 15%.

Concerning the 3rd prop level, all models overestimate the prop forces, where both monitored straight props show the same value of 650kN/m. HSM and Mohr-C models overestimate the measurements by about 33% - SGRM by 57%.

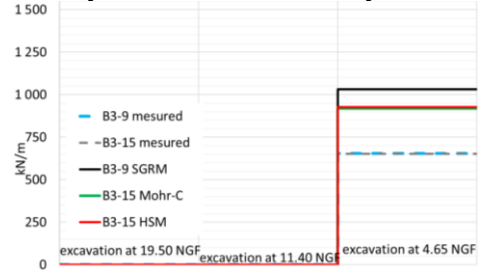

Figure 13. Forces in props at 12NGF

A sum of all three prop levels in comparison to props n°15 measurements gives an overestimation of 42% for HSM, of 31% for Mohr-C and of 27% for SGRM for the final excavation stage.

5 CONCLUSIONS

Thanks to accurate measurements a complete analysis of the inclinometers, prop forces and convergence measurements has been performed. The convergence measurements match the inclinometric displacements at all 3 levels. Inclinometric measurements for the pumping test and all excavation phases were compared with SGRM and FEM calculations.

For the pumping test, a contrast of rigidity can be noticed at the MC and SB soil layers interface. In order to model this rigid behavior below the SB layer, FEM moduli for Mohr-C and HSM were increased (as per §4.3). For SGRM, the subgrade reaction coefficient k_h was determined by adjusting the interaction depth. SGRM gives a better fit than the FEM to the inclinometric measurements.

With regards to the excavation stages, for the FEM models the usual E_M/α factors were chosen (4 for Mohr-C and 2 for HSM models). For the SGRM calculations Schmitt's formula for k_h without any modifications was used. Mohr-C underestimates wall displacements for all construction stages. HSM and SGRM curves show a very good fit for all construction stages below level 25NGF. Above this level HSM and SGRM models slightly overestimate the displacements. The maximum displacements match the inclinometric measurements and fit between both measured curves.

Concerning the prop forces, they were firstly measured by strain gauges then separated into earth and temperature induced forces. Then the earth-induced component was compared to SGRM and FEM models. For the first prop level, the force is overestimated by FEM models and shows a better fit with the SGRM. For the 2nd and 3rd prop level, all models overestimate the prop forces and show a similar behavior, with an increase in prop force as excavation proceeds. SGRM shows the closest calculated forces in comparison to the analyzed section (props n°15).

The back-analysis of Les Ardoines Western pit, which is a 30m deep excavation with a 26m ground water head, shows that: the Mohr-C (with $E = 4 \cdot E_M/\alpha$) slightly underestimates the displacements but shows correct prop forces, both the HSM (with the usual E_M/α factors) as well as the SGRM models (with unmodified Schmitt's formula) are suitable for both wall displacements and prop forces determination.

The authors would like to add that SGRM or FEM methods are only mathematical modeling tools that try to represent reality. Although there can be some value in comparing various numerical models, real practical conclusions can only be drawn by comparing modeling tools with quality in-situ structure's measurements.

6 ACKNOWLEDGEMENTS

The authors thank Horizon's (Soletanche Bachy and Bouygues TP Joint-Venture) monitoring department and Sixense Soldata for every help concerning the measurements provided.

7 REFERENCES

AFNOR 2009 Geotechnical design – retaining structures, NF P 94-282.

Boone S. J., Crawford A. M. (2000). Braced excavations: temperature, elastic modulus and strut loads. *J. Geotech. Geoenv. Eng 126(8),* 718-726.

Serrai K., Plumelle C., Schmitt P. (2005). Analysis of measured deflections of a diaphragm wall in Colombes using finite element calculations. *16th ICSMGE, Osaka.*

Schmitt P. (1995). Méthode empirique d'évaluation du coefficient de réaction du sol vis-à-vis des ouvrages de soutènement souples. *Rev. Fr. de Géotechnique 71, 3-10.*

Twine D., Roscoe H. (1999). Temporary propping of deep excavations – guidance on design. CIRIA C517.